Evaluation of rolling contact fatigue crack path of high strength steel with artificial defects

T. Makino[1], Y. Neishi[1], D. Shiozawa[2], Y. Fukuda[2] and Y. Nakai[2]

[1] Corporate Research & Development Department, Sumitomo Metal Industries, Ltd., JAPAN, makino-tiz@sumitmometals.co.jp
[2]Department of mechanical Engineering, Kobe University, JAPAN

ABSTRACT. *The objectives of the present paper are to clarify the rolling contact fatigue (RCF) crack path of high strength steel with artificial defects by synchrotron radiation micro computed tomography (SR micro CT) imaging and discuss the mechanism of RCF crack propagation by finite element (FE) analysis. As a result, two types of cracks, that is, a vertical crack and a horizontal crack were inspected around the artificial defect by SR micro CT. SIF of horizontal cracks, calculated by FE analysis, became large due to vertical cracks. The interaction of both cracks would appear to dominate RCF crack propagation originated from artificial defects.*

INTRODUCTION

Rolling contact fatigue (RCF) property is a crucial one for mechanical elements subjected to rolling contact, (e.g. bearings, gears, wheels and rails). In particular, properties under pure RCF, that is, without macroscopic slip and under oil lubrication, are influenced by a non-metallic inclusion. The detrimental effect of inclusion on the RCF property has been discussed by many researchers[1-6]. According to previous researches, size, shape, location and composition of inclusion, interface condition between inclusion and surrounding matrix were considered as factors affecting the RCF life.

From the point of view of fracture mechanics, smaller inclusions, high interfacial strength, smaller differences of Young's modulus between an inclusion and a surrounding matrix lead to longer RCF life[1]. On the other hand, from the point of view of metallurgy, transformation of a microstructure of the matrix around the inclusion, a so-called WEA, or a white etching area is considered an influencing factor on RCF life[2]. This research almost entirely focused on the internal inclusion of the spheroidized type (e.g. Al_2O_3).

However, Nagao et al.[3] indicated that stringer type inclusions can be origins of RCF cracks and flaking in the case of disc specimens taken from cross section of steel bars. Moreover, Neishi et al.[4] revealed that, in the case of material which is comprised of a stringer type inclusion perpendicular to the rolling contact surface, the length of inclusion negatively influenced RCF life. In the present paper, in order to discuss the

above result, the RCF property of the material with artificial defects simulating stringer type inclusions is evaluated.

It is known that synchrotron radiation micro computed tomography (SR micro CT) imaging enables detection of inclusions[5] and small cracks. Moreover, an SR micro CT could be used in the observation of RCF crack initiation and propagation from inclusions. The present authors succeeded in detecting small cracks below a flaking damage and around an artificial defect by SR micro CT[6].

The objectives of the present paper are to clarify the RCF crack path of high strength steel with artificial defects by SR micro CT imaging and to discuss the mechanism of RCF crack propagation by finite element (FE) analysis. As a result, two types of cracks, that is, a vertical crack and a horizontal crack were inspected around the artificial defect by SR micro CT. SIF of horizontal cracks, calculated by FE analysis, became large due to vertical cracks. The interaction of both cracks would appear to dominate RCF crack propagation originated from artificial defects.

ROLLING CONTACT FATIGUE TEST

Materials and specimens

Ball-on-disc type RCF tests were conducted under oil lubrication. The material of the disc specimen and ball specimen were induction-hardened 0.55% carbon steel. Table 1 shows the chemical composition of the disc specimen material. The disc specimen was 60mm in diameter and 5 mm in thickness. The diameter of ball specimen was 9.525mm. A ring-shaped region with 35-45mm in diameter on one side of the surface of the disc specimen was induction-hardened. Vicker's hardness of induction-hardened region is *HV*720. A ball rolling track in the RCF test was located in a ring-shaped region. An artificial defect of 15μm in diameter and 200μm in depth was introduced on the ball rolling track of disc specimen by electro-discharge machining. The defect can simulate a stringer type inclusion (e.g. MnS).

Table 1. Chemical composition of material for disc specimen(mass %)

C	Si	Mn	P	S
0.58	0.19	0.78	0.002	0.004

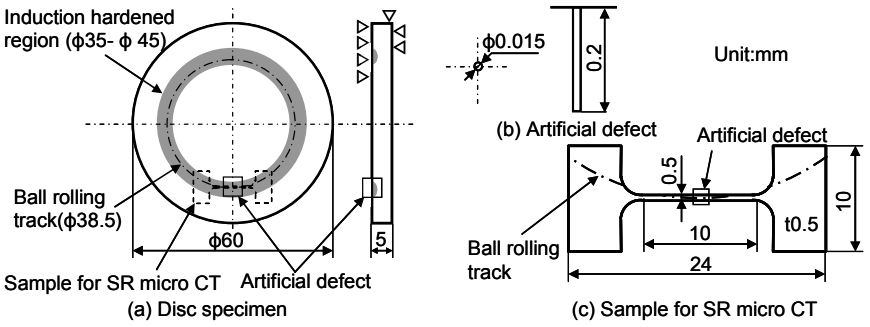

Figure 1. Schematic illustration of disc specimen and sample for SR micro CT.

Test method

Ball-on-disc type RCF tests were conducted by a mori-type RCF test machine. Three balls rolled on one side of the surface of the disc specimen under oil lubrication. A vertical contact force was set so that the Hertzian stress p_{max} became 5.22GPa. The half-width of the contact patch a was then calculated to be 0.346mm. The test stopped at N=1x10^4, 1x10^5, 1x10^6 cycles, where, N represents the number of cycles of rolling contact. The number of cycles to flaking N_f has not been investigated yet, but the result of using a material of similar hardness (bearing steel) indicated N_f=3.20x10^6 cycles under the same test condition. Thus, if the N_f of tested material were the same as the above N_f, the cycle ratio N/N_f at N=1x10^4, 1x10^5, 1x10^6 cycles would be 0.003,0.03,0.3 respectively.

Test results

Fig.2 shows the SEM photos of artificial defect on rolling contact surface after the RCF test. Several small cracks appeared due to the defect, almost perpendicular to the rolling direction and the surface, were found. The cracks are called as "vertical cracks" in the present paper. It can be seen from the figure that the length of the vertical cracks increases with the number of cycles.

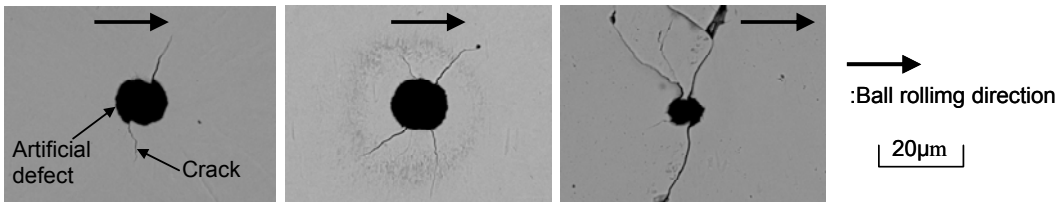

(a) N=1x10^4 cycles (b) N=1x10^5 cycles (c) N=1x10^6 cycles

Figure 2. SEM photos of artificial defect on rolling contact surface after the RCF test.

SR MICRO CT IMAGING OF RCF CRACKS

Test sample

From the disc specimens observed in the previous chapter, a small sample, which included the artificial defect, was taken and inspected by SR micro CT imaging at SPring-8. The shape and size of sample are also shown in Fig. 1(c).

CT imaging method

The CT imaging was carried out at BL19B2 beam line of SPring-8, the brightest synchrotron radiation facility in Japan. Fig. 3 shows the photo and schematic illustration of an CT imaging apparatus. The conditions of measurement were as follows: X-ray energy E=37 keV, sample-detector distance L=0.7 m. The effective pixel size of the detector was from 0.74 to 2.8 μm depending on the magnification of the beam monitor. For a 3-D reconstruction, a set of 900 radiographs of a sample were recorded at rotations of over 180°, where each rotation angle was 0.5°. Slice images were

reconstructed from the series of the projection images by a filtered-back projection algorithm.

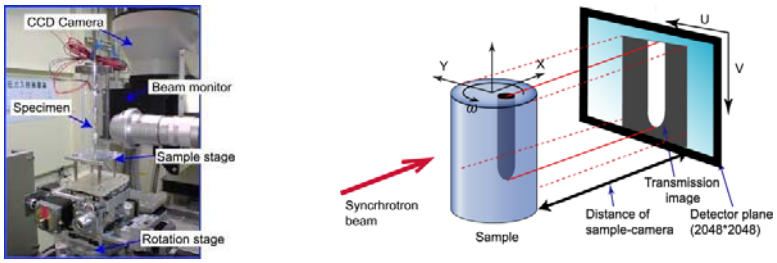

Figure 3. Photo and schematic illustration of CT imaging apparatus.

CT imaging result

Fig. 4 shows the CT images of an artificial defect and cracks. Two types of cracks were inspected around the artificial defect. One is a vertical crack, which propagates perpendicular to the surface along the artificial defect. Another is called a "horizontal crack", which propagates parallel to the surface from some deep positions of the artificial defect. It was determined that both vertical and horizontal cracks initiated before N=1x10^4 cycles. A vertical crack propagated in depth direction and perpendicular to the rolling direction of artificial defect from N=1x10^4 cycles to N=1x10^6 cycles. Horizontal cracks propagated in a horizontal direction simultaneously. The propagated length of a horizontal crack at approximately 150 μm in depth was the largest.

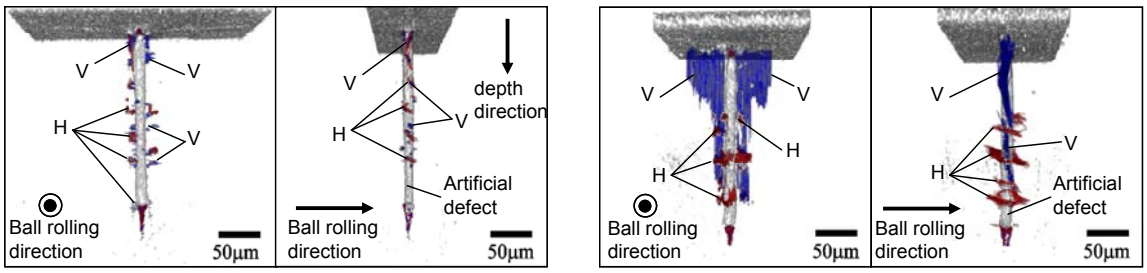

(a) N=1x10^4 cycles (b) N=1x10^6 cycles

Figure 4. CT images of artificial defect and cracks (V:vertical crack, H:horizontal crack).

FINITE ELEMENT ANALYSIS OF RCF CRACKS

FE analysis was carried out in order to calculate the stress states around the defect and the stress intensity factors (SIFs) of the above RCF cracks.

FE modelling and analytical condition

Fig. 5 shows the FE model for the RCF test. The FE model consists of a rectangular block of disc specimen and a hemisphere of ball specimen taking into account the symmetry. The sizes of the cracks are also shown in Fig. 5. Infinite elements were applied for the disc specimen of the rectangular model. Therefore, it was possible to

conduct an accurate analysis using a rectangular model with a fewer number of elements than the disc-shaped model.
A circular hole of the same size as the artificial defect was modelled in a small rectangular section. The section was tied in the centre of the disc specimen model. Models are classified by four types (i.e. with vertical and horizontal crack, without crack, with only vertical crack, with only horizontal crack as shown in Fig. 5(b)-(e)). A finer mesh was applied at the region around the crack tip, the minimum length between nodes being 0.002mm.
Friction coefficients between the ball and disc specimen model and between crack faces were defined as zero taking into account the oil lubrication. The elastic modulus and Poisson's ratio were defined as 205.8GPa and 0.3. Plastic deformation was not considered in the present paper. The vertical force was given to obtain the same Hertzian stress p_{max} (5.22GPa) and half-width of the contact patch a (0.346mm) as the experiment. The ball specimen model moved 8mm across the circular hole and cracks on the disc specimen model.

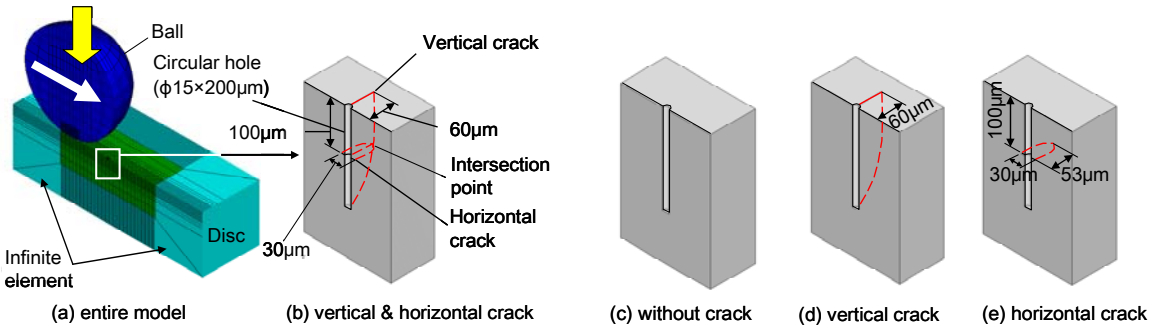

Figure 5. FE models for the RCF test.

FE analysis result

Stress states in the vicinity of the circular hole without crack

Fig. 6 shows the stress states obtained by the model with a circular hole without crack. Note that (a) shows the change in tensile stress in a rolling direction σ_x at the surface edge on the middle line of the hole, and the shear stress in a rolling and depth direction

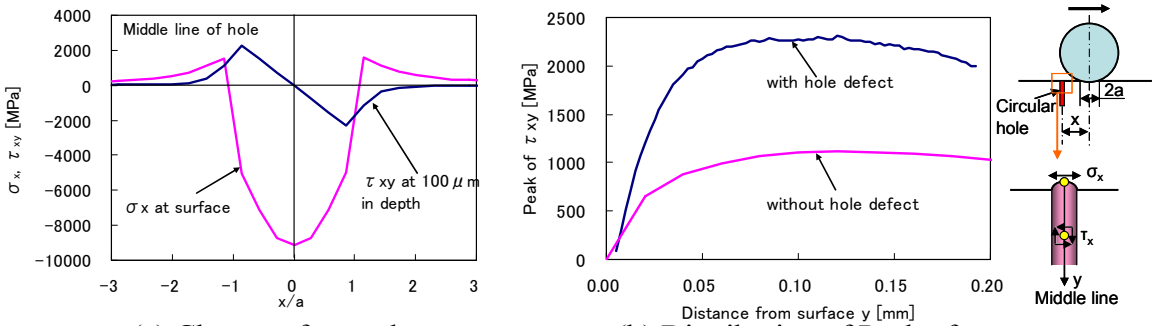

(a) Change of σ_x and τ_{xy} (b) Distribution of Peak of τ_{xy}

Figure 6. Stress states obtained by the model with a circular hole without cracks.

τ_{xy} at 100μm in depth on the same line. Both stresses greatly changed during rolling contact. Also note that (b) shows the distribution of peak of τ_{xy} in depth direction on the middle line of the hole. τ_{xy} calculated by Hertzian theory, equivalent to a model without a hole, is also indicated. The peak of τ_{xy} became twice as big due to the hole defect. It suggests that the defect, like the circular hole, accelerates the RCF crack initiation.

Stress intensity factors of cracks with a circular hole

Fig. 7 shows the change in the SIFs of vertical and horizontal cracks with a circular hole during rolling contact. Some peaks and valleys of SIF appear at various points. The largest peak and valley of SIF is that at mode II SIF K_{II} which occurrs at the tip of an intersection of a vertical crack with a horizontal crack (V-I). Two peaks of mode I SIF K_I at the tip on the surface (V-S) occur before and after rolling contact.

Fig. 8 shows the comparison between the ranges of SIF ΔK obtained from Fig. 7 and the fatigue crack threshold SIFs ΔK_{th}. The mode II and III threshold SIFs ΔK_{IIth} and ΔK_{IIIth} of the tested material have not been investigated yet. However, those using a material of similar hardness (bearing steel) were investigated by some researchers [7]. Assuming that the threshold of SIFs are the same for both tested material and bearing steel, those by Matsunaga et al. [7] are indicated in Fig. 8.

In the figure, the condition in which ΔK is larger than ΔK_{th} leads to the crack propagation. It is possible that the vertical crack propagates at the surface and an intersection in mode II and at the bottom in mode III.

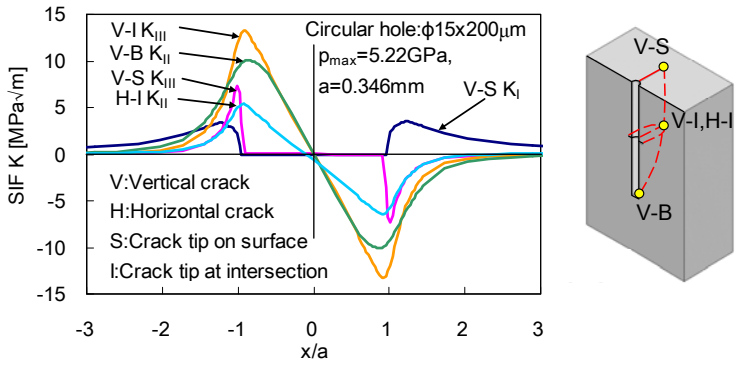

Figure 7. Change in the SIFs of cracks with a circular hole during rolling contact.

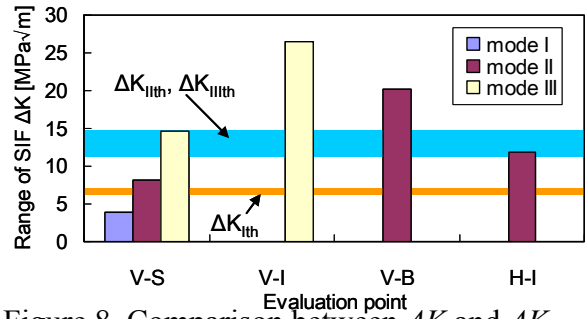

Figure 8. Comparison between ΔK and ΔK_{th}.

DISCUSSION - MECHANISM OF RCF CRACK PROPAGATION

In order to clarify the interaction of vertical and horizontal cracks, two FE models as shown in Fig.5(d) and (e) were calculated. Note that (d) is a model with only a vertical crack, while (e) is a model with only a horizontal crack. The SIFs of vertical cracks were the same in both models with and without horizontal crack. Fig.9 shows the comparison of SIF of horizontal cracks between two models with and without vertical cracks. The mode II SIF of horizontal cracks at an intersection with vertical cracks is larger than that at the same point in the model without vertical cracks. It suggests that a vertical crack accelerates the propagation of a horizontal crack. This would mean that the restraint against shearing deformation of horizontal crack reduces due to vertical cracks. The interaction of both cracks would appear to dominate RCF crack propagation originated from artificial defects.

The process of RCF crack propagation is summarised in Fig. 10. First, vertical cracks initiate at the region close to a surface along an artificial defect due to tension and shear stresses, while simultaneously, horizontal cracks initiate at several depths of the artificial defect due to shear stress. Next, vertical cracks propagate in mode III from the edges at the surface and at intersections with horizontal cracks, and propagate in mode II from the edge at the bottom. Then, horizontal cracks propagate in mode II at intersections with vertical cracks. The preceding process is not calculated, but it is deduced that the horizontal cracks propagate in a rolling direction and towards the surface. Finally, flaking occurs. The hypothesis can also apply to the RCF crack propagation from stringer type inclusions.

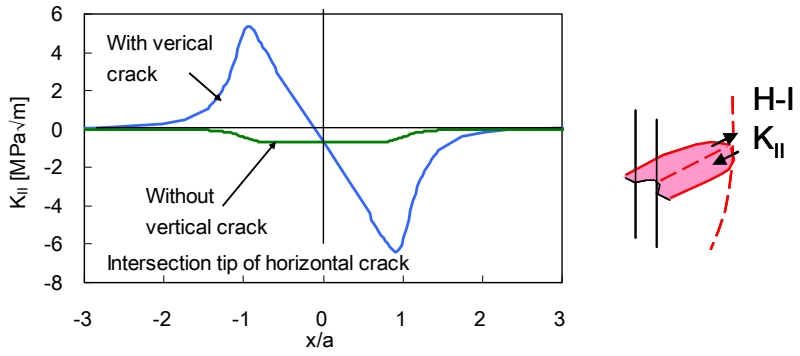

Figure 9. Comparison of SIF of horizontal crack between two models with and without vertical cracks.

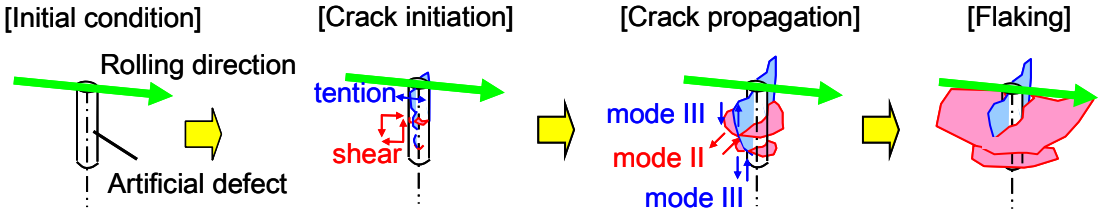

Figure 10. Process of RCF crack propagation.

CONCLUSION

In order to clarify the RCF crack path of high strength steel with artificial defect and discuss the mechanism of RCF crack propagation, SR micro CT imaging and FE analysis were carried out. As a result, the following results were found:

(1) SR micro CT imaging detected the RCF cracks (i.e. vertical and horizontal cracks with artificial defects).
(2) Both vertical and horizontal crack initiated before N=1x10^4 cycles. Vertical cracks propagated in depth direction and perpendicular to the rolling direction of the artificial defect from N=1x10^4 to 1x10^6 cycles. Horizontal cracks propagated in a horizontal direction simultaneously.
(3) Stress states around circular hole during rolling contact were calculated by FE analysis. Tensile and shear stresses generated around the hole. The shear stress was larger than two times of that without the hole.
(4) The SIFs of the above RCF cracks were also calculated by FE analysis. Some peaks and valleys of SIF occur at various points. The largest peak and valley of SIF is that of mode II SIF K_{II} occurring at the tip of an intersection of a vertical crack with a horizontal crack. The range of SIF ΔK_{II} was larger than ΔK_{th} using a material of similar hardness.
(5) In comparison of SIF of horizontal cracks between two models with and without vertical cracks, the mode II SIF of a horizontal crack at an intersection with a vertical crack is larger than that at same point in the model without a vertical crack. It suggests that the vertical crack accelerates the propagation of horizontal cracks.
(6) Interaction of vertical and horizontal cracks described in (5) would appear to dominate RCF crack propagation originated from artificial defects. The hypothesis can also apply to the RCF crack propagation from stringer type inclusions.

The synchrotron radiation experiments were performed at BL19B2 in SPring-8 with the approval of the Japan Synchrotron Radiation Research Institute (JASRI) under proposal numbers of 2011A1859. The authors are grateful for his technical support of Dr. Kentaro Kajiwara (JASRI).

REFERENCES

1. Hashimoto, K. et al. (2011) *Materials and Design* 32 4980–4985
2. Grabulov, A., Ziese, U. et al. (2007) *Scripta Materialia*, 57 (7), 635-638
3. Nagao, M., Hiraoka, K. et al. (2005) *Sanyo Tech. Report* **12**-1, 38-45 (in Japanese)
4. Neishi, Y., Makino, T. et al. (2011) *CAMP-ISIJ* Vol.24-383 (in Japanese)
5. Stienon, A. et al. (2009) *Materials Science and Engineering* A 513–514, 376–383
6. Shiozawa, D., Nakai, Y., Fukuda, Y., Neishi, Y., Makino, T. (2012) *15th International Conference on Experimental Mechanics*
7. Matsunaga, H., Shomura, N., Muramoto, S., Endo, M. (2010) *Fatigue & Fracture of Engineering Materials & Structures* **34**, 72–82